ELSEVIER

Journal of Nuclear Materials 297 (2001) 120–128

journal of nuclear materials

www.elsevier.com/locate/jnucmat

Densification behaviour and sintering kinetics of PuO_2 pellets

T.R.G. Kutty [a,*], K.B. Khan [a], P.V. Hegde [a], A.K. Sengupta [a], S. Majumdar [a], D.S.C. Purushotham [b]

[a] *Radiometallurgy Division, Bhabha Atomic Research Centre, Trombay, Mumbai 400 085, India*
[b] *Nuclear Fuels Group, Bhabha Atomic Research Centre, Trombay, Mumbai 400 085, India*

Received 16 January 2001; accepted 13 May 2001

Abstract

The sintering behaviour of PuO_2 pellets has been studied using a dilatometer in inert, reducing and oxidising atmospheres. The shrinkage rate was found to be maximum for pellets sintered in Ar–8% H_2 atmosphere. The mechanism for the initial stage of sintering was determined using rate controlled sintering (RCS) technique and was found to be volume diffusion for both inert and reducing atmospheres. The activation energy for the initial stages of sintering was found to be 210 and 159 kJ/mol for Ar and Ar–8% H_2 atmospheres, respectively. The mechanism for the sintering in oxidising atmospheres could not be evaluated using RCS technique.

PACS: 81.20.Ev; 61.72.−y; 66.30.Fq

1. Introduction

As part of plutonium utilisation programme, PuO_2 has received considerable attention from the fuel designers and fabricators. The Pu-rich oxide fuel is often considered as the candidate fuel for compact fast reactors as a substitute for the highly enriched uranium (HEU). Also, because of proliferation concerns associated with weapon grade plutonium from dismantled weapons, conversion to non-weapon grade material is considered highly desirable. MOX fuel is one strategy available for using this surplus Pu. MOX fuel production consists of converting Pu metal to PuO_2, which is mixed with depleted UO_2 and pressed into fuel pellets for burning in light water reactors. Since a large amount of Pu has to be converted to PuO_2 powder, there is a need for detailed studies. In this work, the shrinkage behaviour of PuO_2 pellets has been studied using a dilatometer in different types of atmospheres viz. inert, reducing and oxidising. So far, studies have not been reported on the above-mentioned composition in a wide range of atmospheres like Ar, Ar–8% H_2, CO_2 and commercial N_2. Hence, it is felt that the results of this study would be useful to the manufacturers of such fuels.

The phase diagram of plutonium–oxygen system shows the presence of four compounds namely Pu_2O_3, $PuO_{1.52}$, $PuO_{1.61}$ and PuO_2. Below 2100°C, no oxide of higher oxidation state than PuO_2 is found. PuO_2 is the stable oxide of Pu [1–4]. The structure is the fluorite type, isomorphous with UO_2, ThO_2 and CeO_2 and contains four Pu atoms and eight oxygen atoms per unit cell. The lattice dimension and density of PuO_2 are 0.5396 nm and 11.46 g/cm^3, respectively. PuO_2 loses oxygen readily at elevated temperatures in either vacuum, reducing or inert atmospheres. The deviation from stoichiometry is accompanied by the formation of Frenkel defects on the oxygen ion sublattice of the crystal [5,6]. This oxygen deficiency results in the formation of larger Pu^{+3} ions, which causes the unit cell to expand [7]. Unlike UO_2, PuO_2 does not readily incorporate excess oxygen in interstitials and therefore PuO_{2+x} formation has not been reported. PuO_2 can combine with the excess oxygen by adsorption on the surface and the adsorbed oxygen is proportional to the surface area [8]. Considerable amount of work has been

* Corresponding author. Tel.: +91-22 559 2466; fax: +91-22 550 5151.
E-mail address: tkutty@magnum.barc.ernet.in (T.R.G. Kutty).

0022-3115/01/$ - see front matter
PII: S0022-3115(01)00614-6

reported on the shrinkage behaviour of UO_2 and ThO_2 but not much has been reported on PuO_2. For nuclear ceramics, it is reported that the diffusion rate is low under reducing condition and is fast under oxidising condition [6]. Since diffusion is largely dependent on oxygen potential of the sintering atmosphere, it will be worthwhile to determine the effects of such various types as inert (Ar), reducing (Ar–8% H_2) and oxidising (CO_2 and commercial N_2) atmospheres on its sintering behaviour.

The mechanisms of sintering during the initial stage of sintering have been determined using rate controlled sintering (RCS) technique. The rate controlled sintering was first proposed by Palmour et al. [9–11] to describe the sintering where the densification rate is controlled rather than the heating rate. The measurement of this process, using a dilatometer, is very useful for studying the sintering mechanism of powder compacts during the initial stages of sintering. RCS results in the formation of fine grain size pellet, avoids gas entrapment in pores and minimises pore–grain boundary separation [12,13].

2. Rate controlled sintering (RCS)

The principle of RCS is as follows.

The green compact is heated in a dilatometer at a constant heating rate until dl/dt, i.e., slope of the length change vs time curve, becomes larger than a threshold value, at which point the temperature rise is stopped. The shrinkage now takes place under isothermal condition. On completion of sintering at this temperature, which is shown by the smaller dl/dt signal than a second threshold value, the temperature rise is resumed and the process is repeated as shown in Fig. 1.

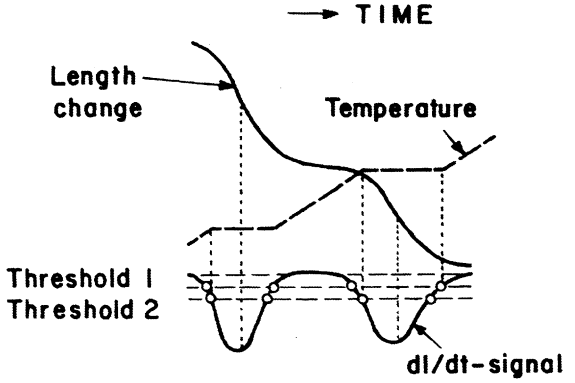

Fig. 1. A schematic drawing of RCS process. The change in length and shrinkage rate (dl/dt) occurring in each isothermal steps is shown. The upper and lower threshold values are shown as threshold 1 and threshold 2, respectively.

The experimental shrinkage curve obtained by dilatometry generally follows an equation of the form [12]

$$\Delta l/l_0 = Y = [K(T)t]^n, \tag{1}$$

where l_0 is the initial length of the sample at the start of the sintering, $K(T)$ is the Arrhenius constant, t is the time and n is a constant whose value depends on the sintering mechanism.

Many models of sintering have been presented and discussed in the literature [14–18]. A sintering model proposed by Johnson [19], in which all the significant mechanisms of materials transport can be identified even though more than one mechanism may be operating simultaneously, has been used in this study. If it is assumed that all the material in the neck comes from grain boundary and if the material transport by surface diffusion, vapour transport are insignificant, then the shrinkage for the first 3.5% can be expressed as [19]

$$Y^{2.06}Y = (2.63\gamma\Omega D_v/kTa^3)Y^{1.03} + (0.7\gamma\Omega bD_b/kTa^4), \tag{2}$$

where is the surface tension, Ω is the vacancy volume, D_v and D_b are the diffusion coefficients for volume and grain boundary, respectively, T is the temperature, a is the particle radius, b is the thickness of the grain boundary and k is the Boltzmann constant.

If only the volume diffusion from grain boundary is operative, then Eq. (2) becomes [19]

$$Y = (5.34\gamma\Omega D_v/kTa^3)^{0.49}t^{0.49}. \tag{3}$$

Similarly for grain boundary diffusion

$$Y = (2.14\gamma\Omega bD_b/kTa^4)^{0.33}t^{0.33}. \tag{4}$$

Eqs. (3) and (4) predict the slopes of 0.49 and 0.33 in a plot of $\ln Y$ vs $\ln t$ for volume diffusion and grain boundary diffusion, respectively.

On differentiating Eqs. (3) and (4) with respect to time, we get

$$\dot{Y} = 0.49(5.34\gamma\Omega D_v/kTa^3)^{0.49}t^{-0.51}, \tag{5}$$

$$\dot{Y} = 0.33(2.14\gamma\Omega bD_b/kTa^4)^{0.33}t^{-0.67}. \tag{6}$$

The slope of the plot of $\ln \dot{Y}$ vs $\ln t$ will be $(n-1)$ from which the sintering exponent 'n' can. be evaluated. From the value of $\dot{Y}$ intercepts, the diffusion coefficient can be evaluated. The variation of $\log D$ with T can be described by an equation of the type

$$D = D_0 \exp(-Q/RT), \tag{7}$$

where D_0 is the pre-exponential factor and Q is the activation energy.

3. Experimental

3.1. Fabrication of green pellet

The green pellets for this study were prepared by the conventional powder metallurgy technique which consists of the following steps:

- milling the plutonium oxide powder in a planetary ball mill for 4 h using tungsten carbide ball,
- pre-compaction,
- granulating the conditioned powders,
- cold pressing of the granulated powders at around 300 MPa into green compact and
- sintering the pressed compact.

The density of green pellets was $52 \pm 1\%$ of theoretical density (TD). To facilitate compaction and to impart handling strength to the green pellets, 1 wt% zinc behenate was added as lubricant/binder during the last hour of milling. The green pellet was around 7 mm long and 4.6 mm in diameter. The characteristics of PuO_2 powders used in this study are given in Table 1.

3.2. Dilatometry

The shrinkage behaviour of the PuO_2 compacts in the various atmospheres was studied using a push rod-type dilatometer. The shrinkage was measured in axial direction. The sample supporter, measuring unit and displaceable furnace of the dilatometer were mounted horizontally. The length change measurements were made by an LVDT transducer, which was maintained at a constant temperature by means of water circulation from a constant temperature bath. The accuracy of the measurement of change in length was within ± 0.1 μm. The temperature was measured using a calibrated thermocouple, which is placed directly above the sample. A small force of 0.2 N was applied to the sample through the push rod. The dilatometric experiments were carried out using a flow rate of 18 l/h and a heating rate of 6°C/min. The impurity contents of the cover gases used in this study are given in Table 2.

The selection of the temperature programme was controlled by a computer via data acquisition system. Correction was applied to the expansion of the system by taking a run under identical condition using a standard sample (POCO graphite, NIST).

For each atmosphere, two pellets were evaluated by dilatometry. One was used to measure the shrinkage from room temperature to 1773 K and the other was used for studying the sintering kinetics using RCS.

Table 1
Characteristics of PuO_2 powders

Property	PuO_2
Oxygen to metal ratio	2.00
Apparent density (g/cm^3)	1.2
Total impurities (ppm)	<1200
Theoretical density, ρ (g/cm^3)	11.46
Surface energy, γ (erg/cm^2)	570[a]
Particle radius,[b] a (A)	97
Specific surface area, S (m^2/g)	13.6

[a] $a = 6/(2\rho Sf)$, where f is the shape factor.
[b] γ_{PuO_2} value is obtained from the relation: $\gamma_{PuO_2}/\gamma_{UO_2} = 0.95$ [48].

3.3. Shrinkage kinetics

For RCS, the temperature programme was modified in such a way that the whole sintering took place between two shrinkage rates as described in Section 2. The heating rate used for RCS was 6°C/min and gas flow rate was 18 l/h. The sintering kinetics of PuO_2 pellets have been evaluated in Ar, Ar–8% H_2, commercial nitrogen and CO_2 atmospheres.

3.4. Characterisation

The PuO_2 pellets sintered in different atmospheres were characterised in terms of their density, oxygen to metal ratio (O/M) and phase content. The O/M ratio was measured thermogravimetrically and the phase content was estimated by X-ray diffractometry. Table 3 gives the typical values of O/M and their density. The X-ray diffraction patterns of the pellets were obtained by using the Cu K_α radiation and graphite monochromator. The typical impurity contents in a sintered pellet are shown in Table 4.

4. Results

Fig. 2 shows the shrinkage behaviour of PuO_2 under various atmospheres such as Ar, Ar–8% H_2, CO_2 and

Table 2
Impurity contents of different sintering atmospheres

Sintering atmosphere	Oxygen (ppm)	Moisture (ppm)	CO_2 (ppm)	CO (ppm)	N_2 (ppm)	Oxides of N_2 (ppm)	Hydrocarbon (ppm)
Argon	4	4	1	1	10	1	1.5
Argon + 8% hydrogen	4	4	1	1	10	1	2
Carbon dioxide	300–400	10	–	5	50	15	2
Commercial nitrogen	400–500	10	50	5	–	–	5

Table 3
Density and O/M ratio of PuO_2 pellet after sintering

Sintering atmosphere	Density (% TD)	O/M ratio
Ar	88	1.96
Ar–8% H_2	89	1.91
CO_2	84	2.00
Commercial N_2	82	2.00

Table 4
Metallic impurities in PuO_2 pellet

Element	Impurity (ppm)
Na	<50
Ca	<120
Al	<10
Mg	<25
Si	<100
Fe	<150
Cr	<70
Co	<5
Ni	<60
Mo	<5
W	<50
B	<0.18

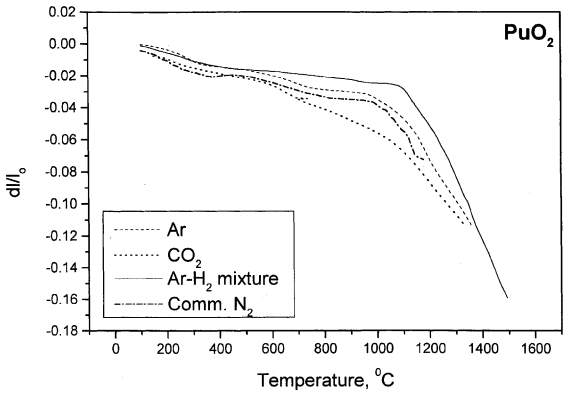

Fig. 2. Shrinkage curves for PuO_2 pellets in Ar–8% H_2, Ar, CO_2 and commercial N_2. The dl/l_0 values are plotted against temperature, where l_0 is the initial length.

commercial N_2. The corresponding shrinkage rates $d(dl/l_0)/dt$ of the above pellet are shown in Fig. 3. It can be seen from Figs. 2 and 3 that the onset of shrinkage occurs at 1050°C in Ar–8% H_2. In Ar it begins at a slightly lower temperature. On the other hand, for CO_2, it occurs at around 600°C. The shrinkage was found to be faster in Ar–8% H_2 than Ar. From the shrinkage rate curves, it was observed that the maximum shrinkage rate occurs for Ar–8% H_2 atmosphere. For the pellets sintered in Ar–8% H_2, large oscillations were noticed above 1100°C in $d(dl/l_0)/dt$ curves.

X-ray diffraction (XRD) pattern of PuO_2 pellets sintered in CO_2 and in commercial nitrogen showed only

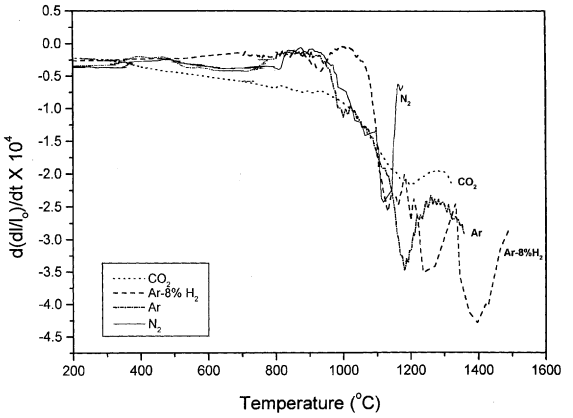

Fig. 3. Shrinkage rate $d(dl/l_0)/dt$ of PuO_2 pellet in Ar–8% H_2, Ar, CO_2 and commercial N_2 atmospheres plotted against temperature.

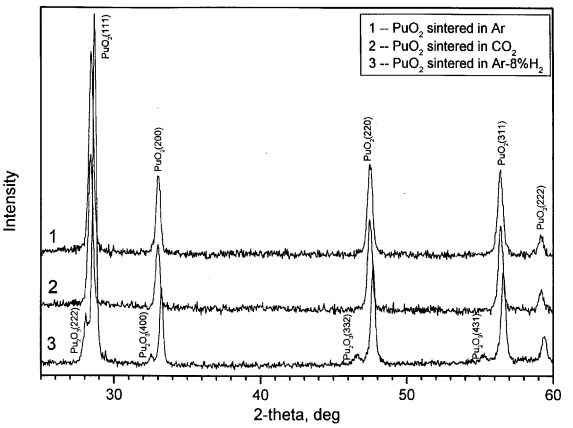

Fig. 4. XRD pattern of PuO_2 pellet sintered in Ar–8% H_2, Ar and CO_2.

single phase. But the diffraction pattern of the PuO_2 pellets sintered in Ar–8% H_2 showed the presence of two phases – one is isostructural with PuO_2 and other is isostructural with bcc α-Pu_2O_3 (see Fig. 4). It was noticed that after sintering PuO_2 in Ar–8% H_2 at a temperature of 1500°C, 14 wt% PuO_2 got converted into bcc Pu_2O_3.

5. Discussion

From the above results, it is clear that PuO_2 sinters well in reducing and inert atmospheres and its sintering characteristics are poor in oxidising atmospheres like CO_2 and commercial nitrogen. We will discuss in detail about these phenomena in the following part of the text.

Sintering is a high temperature process where the individual particles coalesce, giving rise to grain growth, solid solution formation and shrinkage. Sinterability of PuO_2 compacts has been found to depend upon the following factors, namely [20–23]:

1. Pu oxalate calcination temperature,
2. sintering temperature and time,
3. sintering atmosphere and
4. Pu^{+4}/Pu^{+3} ratio.

Sintering is a diffusion controlled process and is rate controlled by the slower moving cation metal atoms. Diffusion in solid itself occurs by the following mechanisms [6]:

1. Vacancy mechanism.
2. Interstitial mechanism.
3. Interstitialcy mechanism.

The point defect model has been used to explain many observed features of diffusion in non-stoichiometric fluorite-type oxide fuels [6]. The point defect model was first developed by Matzke [6,24] and Lidiard [25]. They derived a relation for the temperature dependence of the concentration of vacancies and interstitials in both the oxygen and metal sublattice by solving the anion Frenkel, Schottky and cation Frenkel products. It has been shown that the activation enthalpy for metal diffusion should increase or decrease, respectively, by ΔG_{FO} when passing from MO_2 to MO_{2+x} or MO_{2-x}, respectively, if the metal diffusion occurs via a vacancy mechanism, where ΔG_{FO} is the free energy of formation of oxygen Frenkel defects [6,26–28].

Deviations from stoichiometry produce point defects, most likely oxygen vacancies or metal interstitials in hypostoichiometric compounds and oxygen interstitials or metal vacancies in hyperstoichiometric compounds. The point defects are also created thermally in these materials, provided the temperature is high enough. These defects can exist as single, isolated point defects at low concentration. At higher concentrations, the defects will aggregate into clusters, will become ordered or will be eliminated by the formation of two- or three-dimensional defects such as dislocation loops, shear planes, voids, etc. [26]. For the compounds like actinide oxides, the dominating defect species are often not rate controlling for diffusion-dependent processes. In the fluorite structure, cation mobility is many orders of magnitude smaller than anion mobility. At 1400°C, D^O/D^U has been reported to be greater than 10^5 for UO_2 (depending on x) [27]. Cation diffusion coefficients are, therefore, difficult to measure. Elaborate work has been carried out by Matzke [6,25–28] who has predicted a strong dependence of D^M on x in MO_{2-x}. This was confirmed by experiments on Pu in MO_{2-x}. Since PuO_2 cannot exist in PuO_{2+x} form, we will discuss only about oxygen deficient PuO_2. Three possible mechanisms are suggested for MO_{2-x} which are listed below [6,24,25]:

(a) A vacancy mechanism when $O/M > 1.98$.
(b) An interstitial mechanism for a lower O/M values ($1.95 < O/M < 1.98$).
(c) A cluster mechanism for $O/M < 1.95$.

5.1. Previous work on PuO_2

Extensive research on the sintering behaviour of UO_2–PuO_2 physical mixtures and solid solution formation has been reported. But very little information is available on the sintering behaviour of pure PuO_2. The sintered density of PuO_2 has been evaluated as a function of pressure, temperature and oxalate calcination temperature [20]. A plot of density vs oxygen partial pressure showed a peak for PuO_2 sintered at 1100°C and 1500°C. At a temperature of 1100°C, reduction to $PuO_{1.98}$ occurred at all partial oxygen pressures, while at 1500°C $PuO_{1.98}$ was seen only above an oxygen partial pressure of 10^{-14} atm. Sintered density was also found to be a function of calcination temperature. For a particular oxygen pressure, the sintered density was found to decrease with increase in calcination temperature when this was varied from 300°C to 1050°C [20]. Experiments at a constant oxygen pressure of 10^{-10} atm showed that reduction of PuO_2 begins at about 1300°C and reaches $PuO_{1.70}$ at 2150°C. Extrapolation of these data to the melting point, 2280°C, resulted in $PuO_{1.62}$, which is the composition normally found after melting. The sintering behaviour of PuO_2 in Ar and in hydrogen has been studied by Brett and Russel [23]. The greater densification of PuO_2 in a hydrogen atmosphere may be due to the partial reduction of PuO_2 to alpha Pu_2O_3, which may then serve to promote sintering. Pritchard and Nance [29] have studied the sintering behaviour of PuO_2 in different atmospheres. They have reported that PuO_2 on sintering in Ar showed some reduction of PuO_2 to Pu_2O_3 at around 1250–1350°C, and the amount of Pu_2O_3 increased with increase of temperature. For the pellet sintered in CO_2, no reduction of PuO_2 has been reported. PuO_2 has been found to sinter better in H_2 than in Ar and better in Ar than in CO_2. PuO_2 appears to sinter best in the temperature range of 1300–1600°C when O_2 pressure in the sintering atmosphere is maintained which ensures an O/M of 1.98–2.00. From the standard free energy of formation, an oxygen partial pressure of 3.6×10^{-3} atm is sufficient to stop the formation of Pu_2O_3 at 1650°C [29]. Chikalla [21] has reported that PuO_2 can be reduced to ~50% α-Pu_2O_3 on heating in H_2 at 1650°C or to 25% Pu_2O_3 on just heating at 1450°C. PuO_2 loses a little amount O_2 on heating up to 1100–1200°C in inert or reducing atmosphere but loses O_2 readily at high temperature [30]. The oxygen deficiency results in the formation of large Pu^{+3} ion, which causes the unit cell to expand. Chereau and Wadier [31] have carried out electrical resistivity measurements on PuO_2 and concluded that the major defect

species in PuO_2 are anion vacancies [32,33]. Atlas et al. [34] have shown that the predominant defects in PuO_2 are oxygen vacancies rather than metal interstitials. The measurement of oxygen potential on PuO_2 has shown that it increases with increase in temperature and oxygen content [35–39].

The superior sintering behaviour of PuO_2 in Ar–8% H_2 observed in this study may be associated with the presence of defect structure as PuO_2 gets reduced to Pu_2O_3. This has been confirmed by XRD analysis. The migration energies of Pu^{+3} and Pu^{+4} ions are 4.11 and 5.95 eV, respectively. Hence Pu^{+3} ion can move faster than Pu^{+4} ion resulting a faster diffusion. Therefore formation of Pu_2O_3 in the sample helps in achieving a faster shrinkage rate [40]. In CO_2 and commercial N_2 sinterability of PuO_2 was found to be poor. This may be due to the fact that PuO_2 remains PuO_2 throughout the sintering temperature due to the high oxidising potential of CO_2 and commercial N_2 medium. The O/Pu data for above-mentioned atmospheres are given in Table 3, which shows that the values are very near to the stoichiometric composition. Since no defects are generated, diffusion is slow and this results in poor sintering behaviour. PuO_2 sinters better in Ar than in CO_2 because at high temperature PuO_2 loses its stoichiometry and becomes PuO_{2-x}. This defect structure enhances its sintering behaviour. Our results have been found to agree with the earlier observations reported on PuO_2.

The formation of Pu_2O_3 during the sintering results in the expansion of the unit cell. The ionic radii of Pu^{+3} and Pu^{+4} ions are 0.108 and 0.093 nm, respectively. Thus expansion in the shrinkage curves at around 900–1100°C (see Fig. 2) may be attributed to the formation of large Pu^{+3} ion.

6. Kinetics of sintering

The sintering kinetics have been evaluated for reducing (Ar–8% H_2), inert (Ar) and oxidising (CO_2 and commercial N_2) atmospheres for the initial stages of sintering. The kinetics have been evaluated in a small temperature range of 1031–1092°C for Ar, 1067–1160°C for Ar–8% H_2 and 980–1127°C for CO_2 and N_2 atmospheres. These temperature ranges were chosen from the corresponding shrinkage curves shown in Fig. 2. The H_2O/H_2 and CO/CO_2 ratios of the sintering gases (Ar–8% H_2 and CO_2) used in this study were kept smaller than 10^{-4} during this study.

Fig. 5 shows a typical plot showing the time-dependent variation of dl/l_0 and dl/dt observed in each isothermal step. The parameter 'n' of Eq. (1) is obtained from the slope of $\log \dot{Y}$ vs $\log t$ plot which is shown in Figs. 6 and 7 for Ar and Ar–8% H_2 atmospheres. The value of n obtained for pellets sintered in Ar and Ar–8% H_2 is ~0.50. It was noted that the value of n was around

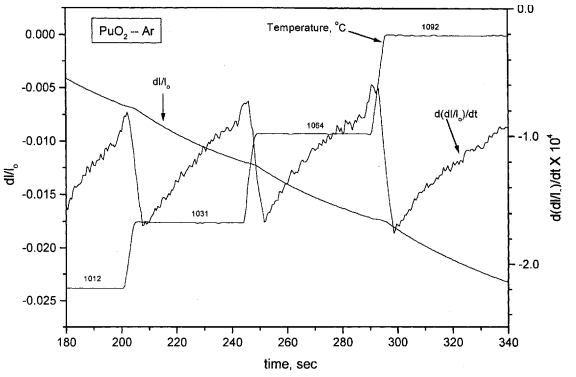

Fig. 5. RCS showing the variation in dl/l_0 and dl/dt occurring in each isothermal step. The atmosphere used was Ar.

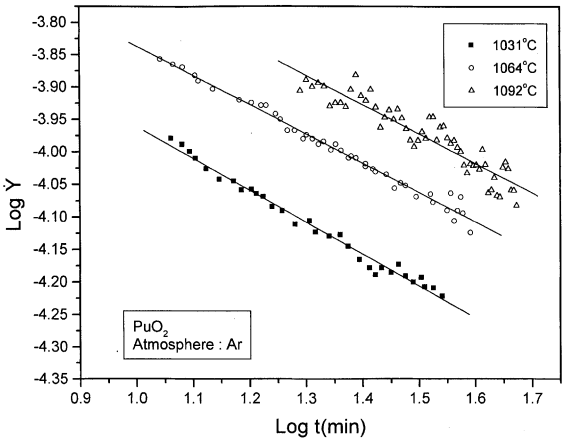

Fig. 6. A plot of $\ln \dot{Y}$ vs $\ln t$ for the pellet sintered in Ar for different temperatures. The slope of this curve will be $(n-1)$ from which the sintering exponent 'n' can be evaluated.

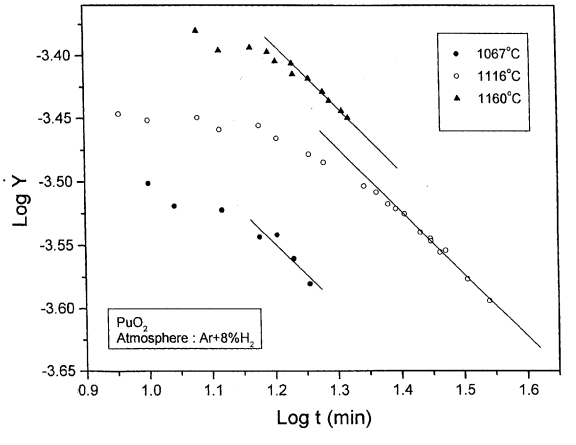

Fig. 7. A plot of $\ln \dot{Y}$ vs $\ln t$ for the pellet sintered in Ar–8% H_2. The slope of this curve will be $(n-1)$ from which the sintering exponent 'n' can be evaluated.

0.7–0.8 during the first few minutes of shrinkage. A similar phenomenon has been reported by Astier et al. [41] for their studies on rutile. This may be due to the fact that the sample may not be reaching thermal equilibrium immediately after attaining the measuring temperature. Hence first several points of the data were discarded and not used in this study. A typical $\log \dot{Y}$ vs $\log t$ plot for CO_2 is shown in Fig. 8. The plot shows that points are all random and hence n could not be determined. Similar observations were also noticed for commercial nitrogen.

Aybers has carried out RCS technique on UO_2, $(U,Th)O_2$, $(U,Pu)O_2$ [42,43] and reported that the mechanism changes with atmosphere used for sintering. He has proposed that the mechanisms during initial stage of sintering are volume and grain boundary diffusion in reducing and oxidising atmospheres, respectively. El-Sayed Ali and Sorensen [44,45] have found $n = 0.32$ in CO_2 atmosphere for $(U,Pu)O_2$ and $n = 0.45$ in reducing atmosphere. Our results agree with this observation for reducing atmospheres.

The diffusion coefficients are calculated from the intercepts in Figs. 6 and 7 using Eqs. (5) and (6). The values of parameters used for this calculation are given in Table 1. The $\ln D$ vs $1/T$ plots for Ar and Ar–8% H_2 atmospheres are given in Figs. 9 and 10, respectively. The activation energies obtained for PuO_2 in Ar and Ar–8% H_2 are 210 and 159 kJ/mol, respectively.

There is no report available in the literature about the activation energy for PuO_2. Hence no comparison is possible. We suggest the following mechanisms on the basis of the above-mentioned observations:

1. Cluster mechanism for pellets sintered in Ar–8% H_2 atmosphere.
2. Interstitial mechanism for Ar atmosphere.

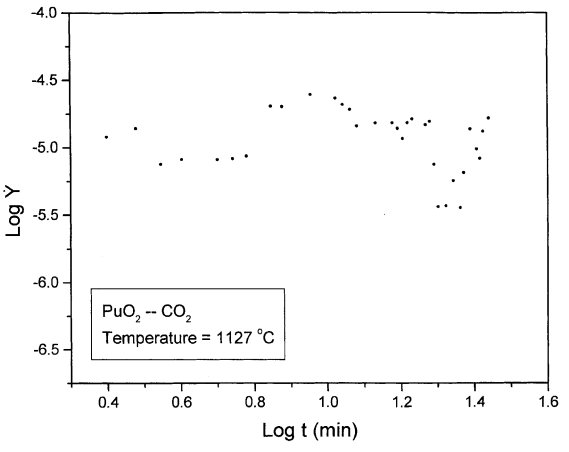

Fig. 8. $\ln \dot{Y}$ is plotted against $\ln t$ for the pellet sintered in CO_2. Unlike the other atmospheres, this curve was found to be random.

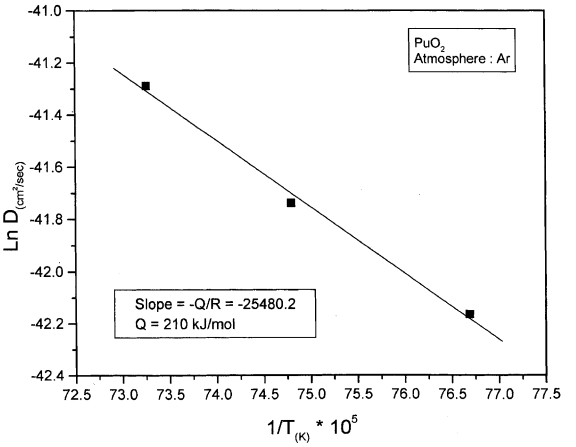

Fig. 9. The Arrhenius plot $\ln D$ vs $1/T$ for PuO_2 pellet sintered in Ar. The slope of this curve will be Q/R from which the activation energy Q can be estimated.

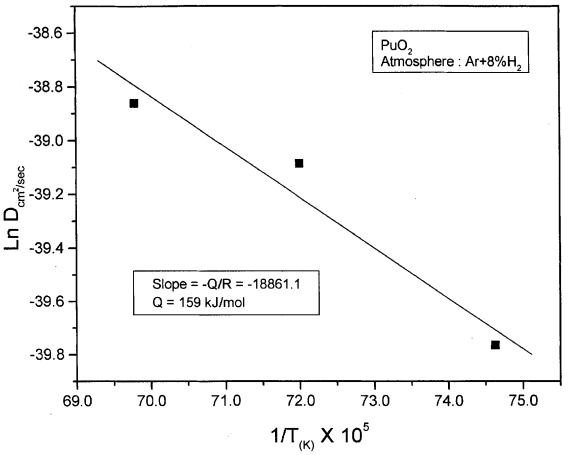

Fig. 10. The Arrhenius plot $\ln D$ vs $1/T$ for PuO_2 pellet sintered in Ar–8% H_2.

6.1. Cluster mechanism

As described earlier, point defect models fail to describe the defect structure of oxide if the degree of non-stoichiometry is large enough [6,26]. Because of their charges, point defects tend to cluster at higher concentration as a result of Coulomb interaction. These defects will become ordered or will get eliminated by the formation of two- or three-dimensional defects such as shear planes, dislocation loops or voids. Cluster formation is well known to occur in MO_{2-x} at large x values. A few pellets of PuO_2 used for RCS studies were checked for their O/M ratio since they have not been fully sintered. The O/M value was found to be 1.94 for Ar–8% H_2 atmosphere. This clearly indicates that the

pellet has considerably deviated from stoichiometry even at ~1250°C and hence defects should cluster. The basic unit for such clusters in MO_{2-x} is a nucleus of known sesquioxide Pu_2O_3. The building unit for the clusters are thus of the type Pu^{+3}–V_o–Pu^{+3}, where V_o is the oxygen vacancy. It is reported that clusters of the type Pu^{3+}–V_o–Pu^{3+} is stable even at 1600°C [5].

Schmitz and Marajofsky [46] have given an interesting alternative to interstitial mechanism to explain the increase in D^{Pu} with decreasing O/M ratio. They proposed an interstitial ring mechanism which results in a change of place of U and Pu atoms. This mechanism suggests that two Pu atoms always remain in close proximity to an oxygen vacancy and the migration of U is in the opposite direction to that of the Pu.

6.2. Interstitial mechanism

The RCS studies have shown that the mechanism for the sintering for the pellet sintered in inert atmosphere (Ar) is volume diffusion and the activation energy for the process is 210 kJ/mol. Heating in argon results in the reduction of PuO_2 to PuO_{2-x}, which results in the formation of metal interstitials [47]. The concentration of these defects increases with increase in temperature as more PuO_2 is getting reduced into PuO_{2-x}. Since very large deviations are not possible in inert atmosphere like Ar, the formation of clusters is ruled out. Hence the most probable mechanism for Ar atmosphere is the interstitial mechanism.

6.3. RCS in oxidising atmospheres

This study also proved that RCS could not be used to determine the sintering kinetics in oxidising atmospheres such as CO_2 and commercial N_2. The O/Pu ratio for pellet sintered in the above-mentioned oxidising atmospheres was found to be 2.00 as shown in Table 3 and hence defect concentration will be much less in these pellets. From our calculation using point defect model, it has been found that the metal interstitial concentration has been reduced by the order of 10^{16} when the sintering atmosphere has changed from Ar–8% H_2 to CO_2 [40]. Hence the net driving force for shrinkage will be very less in these pellets and therefore we could not use RCS process for the evaluation of the kinetics.

7. Conclusions

The sintering behaviour of PuO_2 was studied in various atmospheres such as inert, reducing and oxidising atmospheres. The following conclusions were drawn:

1. Shrinkage begins at a much lower temperature in oxidising atmosphere such as CO_2 and commercial N_2. But the shrinkage rate was the highest for Ar atmosphere.
2. The mechanism for the initial stage of sintering was found to be volume diffusion for both oxidising and reducing atmospheres.
3. The activation energy for sintering was found to be 210 and 159 kJ/mol for Ar and Ar–8% H_2 atmospheres, respectively.
4. The lower activation energy is explained with the help of models available in the literature.
5. Since defect concentration is very less for the oxidising atmospheres like CO_2 and commercial N_2, RCS was found to be ineffective for the evaluation of sintering kinetics.

Acknowledgements

The authors wish to thank Mr H.S. Kamath, Head, Advanced Fuel Fabrication Facility, Tarapur, for his suggestions and comments. They are also grateful to Dr G.C. Jain, Messers T. Jarvis, K. Ravi, P. Sankaran Kutty and G.P. Mishra for their support during the course of this work.

References

[1] H.A. Wriedt, Bull. Alloy Phase Diagram 11 (1990) 184.
[2] T.M. Besmann, J. Nucl. Mater. 144 (1987) 141.
[3] T.D. Chikalla, C.E. Mcneilly, R.E. Skavdahl, Hanford Atomic Production Operation Report, Richland, WA, HW-74802, 1962.
[4] E.R. Gardner, T.L. Markin, R.S. Street, J. Inorg. Nucl. Chem. 27 (1965) 541.
[5] Hj. Matzke, Philos. Mag. A 64 (1991) 1181.
[6] Hj. Matzke, in: T. Sorensen (Ed.), Nonstoichiometric Oxides, Academic Press, New York, 1981, p. 156.
[7] C.R.A. Catlow, J. Chem. Soc., Faraday Trans. 2 (1987) 1065.
[8] E.E. Jackson, M.H. Rand, Atomic energy research establishment, Harwell Report, AERE-R-3636, 1960.
[9] H. Palmour III, M.L. Huckabee, T.M. Hare, in: M.M. Rustic (Ed.), Sintering – New Developments, Elsevier, Amsterdam, 1979, p. 46.
[10] M.L. Huckabee, H. Palmour, Ceram. Bull. 51 (1972) 574.
[11] H. Palmour, D.R. Johnson, in: G.C. Kuczynski, N.A. Hooton, C.F. Gibbs (Eds.), Sintering and Related Phenomena, Gordon and Breach, New York, 1967, p. 779.
[12] D.S. Perera, M.W.A. Stewart, Mater. Forum 20 (1996) 145.
[13] H. Kramer, J. Mater. Sci. Lett. 14 (1995) 778.
[14] D.L. Johnson, T.M. Clarke, Acta Metall. 12 (1964) 1173.
[15] R.L. Coble, J. Am. Ceram. Soc. 41 (1958) 55.
[16] D.L. Johnson, I.B. Cutler, J. Am. Ceram. Soc. 46 (1963) 541.
[17] W.D. Kingery, M. Berg, J. Appl. Phys. 26 (1955) 1205.

[18] L. Berrin, D.L. Johnson, in: G.C. Kuczynski, N.A. Hooton, C.F. Gibbs (Eds.), Sintering and Related Phenomena, Gordon and Breach, New York, 1967, p. 369.
[19] D.L. Johnson, J. Appl. Phys. 40 (1969) 192.
[20] O.J. Wick (Ed.), Plutonium Handbook, p. 250.
[21] T.D. Chikalla, Hanford Atomic Production Operation Report, Richland, Washington, HW-60276, 1959.
[22] L.E. Russell, N.H. Brett, J.D.L. Harrison, J. Williams, A.G. Adwick, Atomic Energy Research Establishment, Harwell Report, AERE-R-3519, 1960.
[23] N.H. Brett, L.E. Russel, Atomic Energy Research Establishment, Harwell Report, AERE-R-3900, 1962.
[24] Hj. Matzke, J. Chem. Soc., Faraday Trans. 86 (1990) 1243.
[25] A.B. Lidiard, J. Nucl. Mater. 19 (1966) 106.
[26] Hj. Matzke, J. Chem. Soc., Faraday Trans. 83 (1987) 1121.
[27] Hj. Matzke, Atomic Energy Canada Ltd. Report, AECL-2585, 1966.
[28] Hj. Matzke, J. Phys. 34 (1973) 317.
[29] W.C. Pritchard, R.L. Nance, Los Alamos Report, Los Alamos, LA-3493, 1965.
[30] T.D. Chikalla, C.E. McNeilly, R.E. Skavdahl, J. Nucl. Mater. 12 (2964) 131.
[31] P. Chereau, J.F. Wadier, J. Nucl. Mater. 46 (1973) 1.
[32] A.S. Bayoglu, R. Lorenzelli, J. Nucl. Mater. 82 (1979) 403.
[33] R.L. Deaton, C.J. Wiedenheft, J. Inorg. Nucl. Chem. 35 (1973) 649.
[34] L.M. Atlas, G.S. Schlehman, D.W. Readey, J. Am. Ceram. Soc. 49 (1966) 624.
[35] T.M. Besmann, T.B. Lindemer, J. Nucl. Mater. 130 (1985) 489.
[36] H. Blank, J. Nucl. Mater. 51 (1974) 269.
[37] T. Sorensen, in: T. Sorensen (Ed.), Nonstoichiometric Oxides, Academic Press, New York, 1981, p. 1.
[38] T.L. Markin, R.J. Bones, E.R. Gardener, Atomic energy research establishment, Harwell Report, AERE-R-4724, 1964.
[39] C.R.A. Catlow, in: T. Sorensen (Ed.), Nonstoichiometric Oxides, Academic Press, New York, 1981, p. 61.
[40] T.R.G. Kutty, P.V. Hegde, K.B. Khan, S. Majumdar, D.S.C. Purushotham, J. Nucl. Mater. 281 (2000) 10.
[41] M. Astier, G. Brula, F. Lecomte, J.P. Reymond, P. Vergnom, in: M.M. Rustic (Ed.), Sintering – New Developments, Elsevier, New York, 1979, p. 150.
[42] M. Aybers, J. Nucl. Mater. 226 (1995) 27.
[43] M. Aybers, J. Nucl. Mater. 210 (1994) 73.
[44] M.El. Sayed Ali, O.T. Sorensen, J. Therm. Anal. 25 (1982) 175.
[45] M. El Sayed Ali, O.T. Sorensen, in: B. Miller (Ed.), Proc. 7th International Conference on Thermal Analysis, Wiley, New York, 1982, p. 344.
[46] F. Schmitz, A. Marajofsky, Thermodynamics of Nuclear Materials 1974, vol. 1, IAEA, Vienna, 1975, p. 467.
[47] T.R.G. Kutty, P.V. Hegde, R. Keswani, K.B. Khan, S. Majumdar, D.S.C. Purushotham, J. Nucl. Mater. 264 (1999) 10.
[48] D.A. Mortimer, AERE Report, AERE- 751, 1974.